Inorganic Chemistry

Article

pubs.acs.org/IC

Electronic Spectra and Crystal-Field Analysis of Europium in Hexanitritolanthanate Systems

Peter A. Tanner,*[,†] Wenyu Li,[‡] and Lixin Ning[§]

[†]Faculty of Physics and Optoelectronic Engineering, Guangdong University of Technology, Guangzhou 510006, People's Republic of China

[‡]Department of Biology and Chemistry, City University of Hong Kong, Tat Chee Avenue, Kowloon, Hong Kong S.A.R., People's Republic of China

[§]Department of Physics, Anhui Normal University, Wuhu, Anhui 241000, People's Republic of China

Supporting Information

ABSTRACT: The luminescence spectra of Eu^{3+} at a T_h point-group site in the hexanitritolanthanate systems $Cs_2NaEu(^{14}NO_2)_6$, $Cs_2NaEu(^{15}NO_2)_6$, $Rb_2NaEu(^{14}NO_2)_6$, $Cs_2LiEu(^{14}NO_2)_6$, and $Cs_2NaY(^{14}NO_2)_6$:Eu^{3+} have been recorded between 19 500 and 10 500 cm^{-1} at temperatures down to 3 K. The spectra comprise magnetic-dipole-allowed zero phonon lines, odd-parity metal−ligand vibrations, internal anion vibrations, and lattice modes, with some weak vibrational progressions based upon vibronic origins. With the aid of density functional theory calculations, the vibrational modes in the vibronic sidebands of transitions have been assigned. The two-center transitions involving NO_2^- stretching and scissoring modes are most prominent for the $^5D_0 \rightarrow {}^7F_2$ hypersensitive transition. The onset of NO_2^- triplet absorption above 20 000 cm^{-1} restricts the derived Eu^{3+} energy-level data set to the ^7F_J (J = 0−6) and $^5D_{0,1}$ multiplets. A total of 21 levels have been included in crystal-field energy-level calculations of Eu^{3+} in $Cs_2NaEu(NO_2)_6$, using seven adjustable parameters, resulting in a mean deviation of ∼20 cm^{-1}. The comparison of our results is made with Eu^{3+} in the double nitrate salt. In both cases, the fourth-rank crystal field is comparatively weaker than that in europium hexahaloelpasolites.

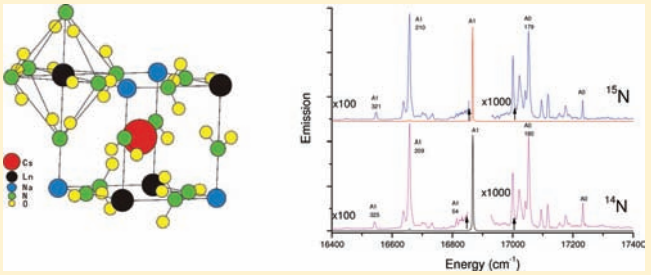

INTRODUCTION

The hexanitritolanthanates $Cs_2NaLn(NO_2)_6$ are attractive candidates for the study of the crystal field of lanthanide ions, Ln^{3+}. The crystal structures[1] show that Ln^{3+} ions are 12-coordinated to a fan of six NO_2^- ions, with the unusual T_h point-group symmetry. By contrast to NO_2^- (hexanitro) complexes of transition-metal ions,[2] the ligand exhibits bidentate oxygen coordination to Ln^{3+}.

One motivation for the present study concerned the crystal field in these complexes. In the hexahaloelpasolites Cs_2NaLnX_6 (X = Cl, F), where the Ln^{3+} ion is octahedrally coordinated, two independent crystal-field parameters, B_{40} and B_{60}, are required in the expression for the O_h-symmetry crystalline-field potential. A third parameter, B_{62}, needs to be added when the lanthanide ion is situated at a site of T_h symmetry, as in the present case, due to the 2-fold rotational symmetry along the principal cubic axes. The sign of B_{62} has no influence on the energies of the levels. From variable-temperature studies of the magnetic susceptibilities of $Cs_2NaLn(NO_2)_6$, Roser and Corruccini[3] concluded that the crystal-field splittings of rare-earth energy levels are generally smaller than those of the Cs_2NaLnX_6 systems. It was suggested that this could be due to the larger lattice constants in the hexanitrito series (ca. 11 Å, vs 10 Å for the $Cs_2NaLnCl_6$ series) or the greater delocalization of charge for NO_2^-, compared with Cl^-. It was also noted[3] that the susceptibilities were consistent with the assumption that the magnitude of B_{40} is much greater than that of B_{60}. We found from studies of the $Cs_2NaLnCl_6$ systems that B_{40} is about 10 ± 2 times greater than B_{60}. However, in our recent parametrization of the energy levels of Pr^{3+} deduced from the electronic spectra of $Cs_2NaPr(NO_2)_6$,[4] it turned out that the magnitude of B_{40} is less than twice that of B_{60} and only 0.56 times that of the parameter B_{62}. These changes modify the energy-level structure of the rare-earth ions in the $Cs_2NaLn(NO_2)_6$ systems, and hence the electronic band positions and intensities, as well as the magnetic properties.

Studies of the vibrational spectra of Ln^{3+} hexanitrito systems have been reported by Barnes and Peacock[5] and Bünzli et al.,[6] and these are subsequently discussed. The highest-energy vibrations correspond to NO_2^- stretching modes, in the region of 1240−1340 cm^{-1}. Detailed vibrational assignments are lacking, however, and this necessitated a theoretical treatment of the vibrational behavior of the $M_2^{I}M^{II}Eu(NO_2)_6$ systems (M^{I} and M^{II} univalent cations) by density functional theory (DFT) because the electronic spectra are mainly vibronic in nature.

Because T_h point-group symmetry is rather unusual for the site symmetry of lanthanide ions, the character table for this point group and the selection rules for magnetic-dipole (MD)

Received: October 27, 2011
Published: February 15, 2012

   dx.doi.org/10.1021/ic202330h | Inorg. Chem. 2012, 51, 2997−3006

and vibronic transitions in the electronic spectra of $4f^N$ (N = even) systems are included in the Appendix. All crystal-field levels of the $4f^6$ configuration transform as gerade representations so that the subscript "g" has been omitted throughout this work when they are referred to. The 3- and 2-fold energy-level degeneracies of the O_h point group are preserved in T_h. However, the transition selection rules are slightly less restrictive than those for the O_h point group, for instance, because both T_1 and T_2 (O_h) irreps transform as T (T_h). The parity selection rule forbids the presence of pure and forced electric-dipole electronic transitions for lanthanide ions of both point groups, with the electric-dipole intensity reserved only for vibronic transitions. The T_2–A (O_h) transitions transform as T–A (T_h) and are potentially MD-allowed in the latter point group.

Another motivation for the study of the hexanitrito complexes of lanthanide ions concerned the possibilities of up- or downconversion for the NO_2^- and Ln^{3+} electronic transitions. However, with the use of near-IR laser-diode excitation into Yb^{3+} electronic energy levels, we were unable to observe emission from NO_2^- in $Cs_2NaYb(NO_2)_6$, although the energy of the triplet state is roughly double that of $Yb^{3+2}F_{5/2}$. Upconversion was also not observed for the Ln = Er^{3+} system. By contrast, as demonstrated herein for Ln = Eu, excitation into NO_2^- triplet vibronic levels in the ultraviolet spectral region provides a broad-band downconversion excitation path for the red emission of Eu^{3+}.

The structure of this paper is as follows. Following an account of the experimental methods, a brief report of the theoretical basis for the vibrational and crystal-field calculations is presented. The calculation results for vibrational frequencies are compared with experimental data, and a general survey of the room temperature luminescence and low-temperature absorption spectra is then made. This is followed by analysis of the emission spectra of Eu^{3+} in various hexanitrito systems. The derived energy levels are then fitted by a parametrized Hamiltonian. Finally, some conclusions are made from the results of this study.

EXPERIMENTAL SECTION

Crystals of compositions $Rb_2NaEu(NO_2)_6$, $Cs_2LiEu(NO_2)_6$, $Cs_2NaEu(NO_2)_6$, and $Cs_2NaY(NO_2)_6$:Eu^{3+} (1 atom %) were synthesized by using the corresponding hexachloroelpasolites as starting materials. The latter were prepared from RbCl, LiCl, CsCl, NaCl, and Eu_2O_3 [and Y_2O_3] (Strem Chemicals, 99.999%). Then, following the addition of a $NaNO_2$ solution, the aqueous solutions were kept in the refrigerator for crystallization at 4 °C. After a few days, transparent crystals were obtained, removed from the mother liquor, and dried. Unless otherwise indicated, the atomic mass number of nitrogen is 14, throughout the following. The ^{15}N crystals were prepared by using sodium nitrite-^{15}N (99%: Shanghai Research Institute of Chemical Industry).

IR Nujol mull spectra were recorded at room temperature in the range from 400 to 4000 cm^{-1} using a Nicolet FT-IR instrument with resolution 4 cm^{-1}. The 95 K IR spectrum of $Cs_2NaEu(NO_2)_6$ was recorded using a Specac cell with KBr windows. FT-Raman spectra were recorded at room temperature by a Perkin-Elmer Spectrum 2000 spectrometer using a resolution of 4 cm^{-1}. Electronic emission spectra were recorded at a resolution of between 2 and 4 cm^{-1} by an Acton 0.5 m monochromator having a 1200 grooves mm^{-1} grating blazed at 500 nm and a back-illuminated SpectruMM CCD detector, using an Optical Parametric Oscillator (Panther) pumped by the third harmonic of a Surelite Nd:YAG pulsed laser. The sample was housed in an Oxford Instruments closed-cycle cryostat or an Oxford Instruments Optistat CF continuous-flow top-loading static cryostat.

THEORETICAL SECTION

DFT Calculations on Vibrational Frequencies. The first-principles calculations were carried out using the DFT plane-wave code VASP[7] with the GGA-PBE exchange-correlation functional.[8] Because of the complexity associated with the $4f^6$ electrons of Eu^{3+}, the calculations were restricted to the closed-shell systems $Cs_2NaLn(NO_2)_6$, $Cs_2NaLa(^{15}NO_2)_6$, and $Rb_2NaY(NO_2)_6$. The $5s^25p^66s^1$ ($4s^24p^65s^1$) electrons on Cs (Rb), the $2p^63s^1$ electrons on Na, the $5d^16s^2$ ($4s^24p^24d^15s^2$) electrons on La (Y), the $2s^22p^3$ electrons on N, and the $2s^22p^4$ electrons on O were treated as valence electrons in the calculations. The interaction between the valence electrons and the core was described using the projected augmented wave (PAW) method.[9,10]

The N and O atoms in $A_2NaM(^{14,15}NO_2)_6$ (A = Cs, Rb, M = La, Y) are located at sites with C_{2v} and C_s point symmetries, respectively, which depend on one and two internal parameters, with the calculated and experimental[1] values being listed in Table 1. As a first step in determining the vibrational frequencies, the internal parameters of the primitive cells were relaxed at the experimental lattice constants until the total forces on each ion were less than 10^{-4} eV $Å^{-1}$. The Γ-point vibrational frequencies were then computed by a finite-difference approach with a step size of 0.02 Å. To ensure converged results, the cutoff energy for the plane-wave basis was set to 400 eV, the criterion for electronic minimization was 10^{-6} eV, and a 6 × 6 × 6 Monkhorst–Pack **k**-point grid (38 irreducible **k** points) was used to sample the Brillouin zone.

Table 1. Calculated Internal Parameters for the $Cs_2NaLa(^{14,15}NO_2)_6$ (a = 11.38 Å) and $Rb_2NaY(NO_2)_6$ (a = 10.90 Å) Crystals

		N (at C_{2v} sites)	O (at C_s sites)	
		z	y	z
$Cs_2NaLa(^{14}NO_2)_6$	calcd	0.2783	0.0941	0.2174
$Cs_2NaLa(^{15}NO_2)_6$	calcd	0.2783	0.0941	0.2174
	exptl[1]	0.2800	0.1000	0.2270
$Rb_2NaY(^{14}NO_2)_6$	calcd	0.2767	0.0978	0.2128
	exptl[1]	0.2700	0.0940	0.2220

Energy-Level and MD Transition Intensity Calculations. The calculation of the electronic energy levels for the $4f^6$ configuration employed the f-shell programs of Prof. M. F. Reid, in which the energy levels were derived by simultaneous diagonalization of various parametrized interaction Hamiltonians. The calculations employed the full basis set of 295 multiplet terms of Eu^{3+}. The details of such calculations can be found in ref 11. The values of the interaction parameters, including F^k (k = 2, 4, 6) for Coulomb interaction between the 4f electrons, ζ(4f) for the spin–orbit interaction, and B_{kq} for the crystal-field interaction, were varied simultaneously within certain allowed ranges and optimized until the best agreement was obtained between the calculated and observed energy levels. The values of the configuration interaction parameters α, β, and γ, as well as the k = 0 magnetic interaction parameters M^k ($M^2 = 0.56M^0$; $M^4 = 0.38M^0$), were held constant and equal to those of the elpasolite compound $Cs_2NaEuCl_6$.[12,13] In order to test the sensitivity of the energy-level calculations, two different approaches were instigated. It is well-known that the derived parameters from energy-level fits of the lanthanide systems are subject to change when different multiplet terms are included in the fits. Previous calculations of the energy levels of $Cs_2NaEuCl_6$ have included 27[12] or 77[13] energy levels in the fitting, hence giving different parameter values. We have

dx.doi.org/10.1021/ic202330h | Inorg. Chem. 2012, 51, 2997–3006

Table 2. Calculated Vibrational Frequencies (cm^{-1}) for $M^{I}_2M^{II}Ln(^{x}NO_2)_6$[a]

		calculation				300 K experiment[c]			
symm	type (major contribution)[b]	$Cs_2NaLa(^{14}NO_2)_6$	$Cs_2NaLa(^{15}NO_2)_6$	$\Delta(^{14,15}N)$	$Rb_2NaY(^{14}NO_2)_6$	$Cs_2NaEu(^{14}NO_2)_6$	$Cs_2NaEu(^{15}NO_2)_6$	$Rb_2NaEu(^{14}NO_2)_6$	$Cs_2LiEu(^{14}NO_2)_6$
A_g	N−O sym str	1325	1302	23	1339	1336	1312	1341	1336
T_u	N−O antisym str	1318	1294	24	1330	*1328*	*1308*	*(1341)*	*1333*
E_g	N−O str	1316	1292	24	1327				
T_g	N−O str	1244	1219	25	1268	1254	1230	1259	1254
T_u	N−O str	1228	1203	25	1249	*1243*	*1219*	*1238*	*1236*
A_g	NO_2 sciss	814	810	4	831	845	841	843	845
E_g	NO_2 sciss	804	800	4	822	838	835	837	839
T_u	NO_2 sciss	804	799	5	820	*831*	*832*	*833*	*835*
T_u	NO_2 wag	292	288	4	347	*321*			*(314)*
T_g	NO_2 wag	288	283	5	342	323	317	320	323
A_g	Ln−O sym str	221	218	3	255	239	237	(253)	239
T_u	Ln−O antisym str	210	208	2	251	*222, 248*		*(266)*	*(240)*
T_g	NO_2 rock	192	192	0	210	192	193	192	190
T_u	NO_2 rock	183	183	0	202	*179*			
A_u	NO_2 twist	175	175	0	201				
E_g	Ln−NO_2 str	169	166	3	195	162	160	160	162
T_u	Ln−NO_2 str	157	155	2	167	*162*			
T_g	NO_2 bend	133	133	0	162	138			
T_u	Ln−NO_2 bend	122	121	1	148	*140*			
T_g	Ln−NO_2 bend	112	113	−1	138	116			
E_u	NO_2 bend	100	100	0	114				
T_u	Ln−NO_2 bend	92	91	1	109				
T_g	Ln−NO_2 rot	65	66	−1	64	77			
T_u	M^{I}−LnNa(NO_2) trans	55	55	0	58	*69*			
T_g	M^{I} trans	46	46	0	56				
T_u	acoustic	2	2	0	2				

[a]Experimental Raman (infrared) data are in normal (italics) font. The far-IR and low-energy Raman data for $Cs_2NaEu(NO_2)_6$ are taken from the report of Bünzli et al. [b]symm = symmetry; sym = symmetric; str = stretch; antisym = antisymmetric; sciss = scissor; rot = rotational; trans = translational. [c]Values in italics are from 300 K IR spectra. Other entries are from 300 K Raman spectra.

therefore employed the parameter values from both calculations when assigning fixed parameter values herein for $Cs_2NaEu(NO_2)_6$. The calculations are labeled A (using fixed parameter values from ref 12) and B (with fixed parameter values from ref 13).

The unpolarized intensity I_{if} of the MD transition from the initial $|f^6\Gamma_i\rangle$ to the final $|f^6\Gamma_f\rangle$ levels may be expressed as

$$I_{if} \propto \bar{\nu}_{ij}{}^3\mu_B{}^2 \sum_{q,\gamma_i,\gamma_f} |\langle f^6\Gamma_i\gamma_i|(L + 2S)_q|f^6\Gamma_f\gamma_f\rangle|^2$$

where $\bar{\nu}_{ij}$ is the transition wavenumber, μ_B is the Bohr magneton, and the summation is over the polarization q (q = 0, ±1) and the components γ of the initial and final levels. The MD moments can be calculated using the formula described in ref 14 by employing the electronic wave functions from the energy-level calculations.

In view of the extensive computer time involved when using the full basis of *SLJ* multiplets of Eu^{3+}, some simplifications were made in the MD intensity calculations. When the wave functions from calculation B are employed, the number of multiplet terms utilized in the intensity calculations was restricted to the lowest 150. The wave function of each crystal-field state was restricted to multiplet contributions >0.1%.

RESULTS AND DISCUSSION

Vibrational Data. There are 66 vibrational degrees of freedom in the $Cs_2NaLn(NO_2)_6$ crystal, and some vibrational modes are doubly or triply degenerate. The $Ln(NO_2)_6{}^{3-}$ moiety modes transform as $3A_g + A_u + 3E_g + E_u + 5T_g + 8T_u$ (T_h). The description of the vibrational motions is included in Table 2 (column 2), and these are categorized as internal NO_2^- modes, Ln−ligand modes, and external (lattice) modes, although many vibrations are of mixed character. Using the optimized structures in Table 1, the Γ-point vibrational frequencies for the primitive cells of the hexanitrito systems were computed. Columns 3, 4, and 6 in Table 2 list the calculated vibrational frequencies for $Cs_2NaLa(NO_2)_6$, $Cs_2NaLa(^{15}NO_2)_6$, and $Rb_2NaY(NO_2)_6$, respectively. In Table 2, the N−O stretching vibrations (1203−1339 cm^{-1}) are located at highest energy, and there is a gap of ~500 cm^{-1} below the NO_2^- scissoring (799−831 cm^{-1}) vibrations to the lower-energy modes. The symmetric and antisymmetric Ln−ligand (O) vibrational energies are calculated to be about 80% of the values for the Ln−ligand (Cl) modes. Column 5 in Table 2 lists the calculated $^{14}N-^{15}N$ frequency shifts for the vibrational modes of $Cs_2NaLa(NO_2)_6$, and these are ~25 cm^{-1} for the N−O stretching modes, ~5 cm^{-1} for NO_2^- scissoring, and rather less for lower-energy vibrations. Experimental internal parameters are not available for $Rb_2NaLa(NO_2)_6$ so that the effects upon vibrational frequencies resulting from replacement of Cs by Rb were investigated for $Rb_2NaY(NO_2)_6$ (where also the substitution of La by Y is expected to lead to higher vibrational frequencies). Column 6 in Table 2 shows that the percentage increases in vibrational energy are rather greater for the lower-energy vibrations.

dx.doi.org/10.1021/ic202330h | Inorg. Chem. 2012, 51, 2997−3006

Columns 7−10 in Table 2 provide a comparison with the experimental data for several Eu^{3+} systems. The Raman and IR spectra of $Cs_2NaEu(NO_2)_6$ (with ^{14}N and ^{15}N) above 800 cm^{-1} have been presented previously,[15] and the corresponding spectra for $Rb_2NaEu(NO_2)_6$ and $Cs_2LiEu(NO_2)_6$ are shown in Figure 1a. The 95 K IR spectrum of $Cs_2NaEu(NO_2)_6$ shows features above 500 cm^{-1} at 837, 1242, and 1335 cm^{-1}, with weaker bands corresponding to combination modes.

With respect to these comparisons, it was found from the calculations for $Cs_2NaPr(NO_2)_6$[4] that the calculated 4f-in-valence frequency values >800 cm^{-1} (i.e., the NO_2^- scissoring and stretching) were all larger than the corresponding 4f-in-core values, while for the lower frequency vibrations, the trend was reversed, except for the last two vibrations. The corresponding Eu^{3+}-in-valence frequencies have not been computed because of the enormous computer time required. The experimental assignment of bands in the IR and Raman spectra in Table 2 is based upon the selection rules that A_g, E_g, and T_g vibrations are Raman-active, whereas only T_u modes are IR-active. Then, the vibrational energies show a one-to-one correspondence in decreasing order with calculation, except for the reported IR band at 222 cm^{-1}.[6] This feature is assigned to another component of the Pr−O antisymmetric stretch, either as the transverse optical mode or, more likely, involving a Fermi resonance. The assignments for the T_u NO_2^- rock and lower-energy vibrations have been modified from those given for $Cs_2NaPr(NO_2)_6$,[4] where fewer IR and Raman bands have been reported. IR bands near 180, 140, 100, and 70 cm^{-1} were reported for other $Cs_2NaLn(NO_2)_6$ (Ln = La, Pr, Nd, Ho) systems by Barnes and Peacock.[5] Whereas three of these energies are fairly similar to those given by Bünzli et al.,[6] a feature is listed by the former authors at ∼100 cm^{-1}[5] instead of at 162 cm^{-1}.[6] In view of this, the assignments must be regarded as tentative for the low-energy modes in Table 2.

As noted previously, the NO_2^- wag and N−O stretching modes exhibit slight increases with decreasing Ln^{3+}(VI) ionic radius across the lanthanide series. However, the frequencies of NO_2^- modes do not differ greatly from those encountered in simple ionic nitrite compounds, such as $NaNO_2$.

Survey of Electronic Spectra: Room Temperature Emission and Low-Temperature Absorption Spectra of $Cs_2NaEu(NO_2)_6$. Figure 1b shows a survey of the room temperature emission spectrum of $Cs_2NaEu(NO_2)_6$ excited at 438 nm. It is dominated by the MD-allowed $^5D_0 \rightarrow {}^7F_1$ transition at 16900 cm^{-1}. The same spectrum can be excited by other ultraviolet radiation wavelengths that do not correspond to $4f^6-4f^6$ Eu^{3+} absorption bands, so that energy transfer from the ligand to the metal ion is evident. The room temperature excitation spectrum is presented in the Supporting Information (Figure S3). No emission from ^5D_J (J = 3, 2, 1) is apparent. This is partly due to the onset of NO_2^- absorption above 20 000 cm^{-1} (Figure 1c) and also to the nonradiative span of the $^5D_1-{}^5D_0$ energy gap by two NO_2^- phonons. The features at ∼15 000 cm^{-1} in Figure 1b are due to vibronic transitions of the $^5D_0 \rightarrow {}^7F_2$ sideband and are further discussed in the low-temperature spectral analysis.

The inset in Figure 1b shows that the $^5D_0$ luminescence decay is monoexponential with 1 lifetime of 0.25 ms. Because the 4.2 K lifetime, as measured by Bünzli et al.,[6] is 10.6 ms, the considerable difference at room temperature is due to the increase in the nonradiative rate of $^5D_0$. The energy gap $^5D_0-{}^7F_6$ is ∼12 250 cm^{-1}, so that for this pathway, the nonradiative decay rate is negligible. An alternative deactivation mechanism involves back-transfer to the NO_2^- triplet state, and this will be investigated later.

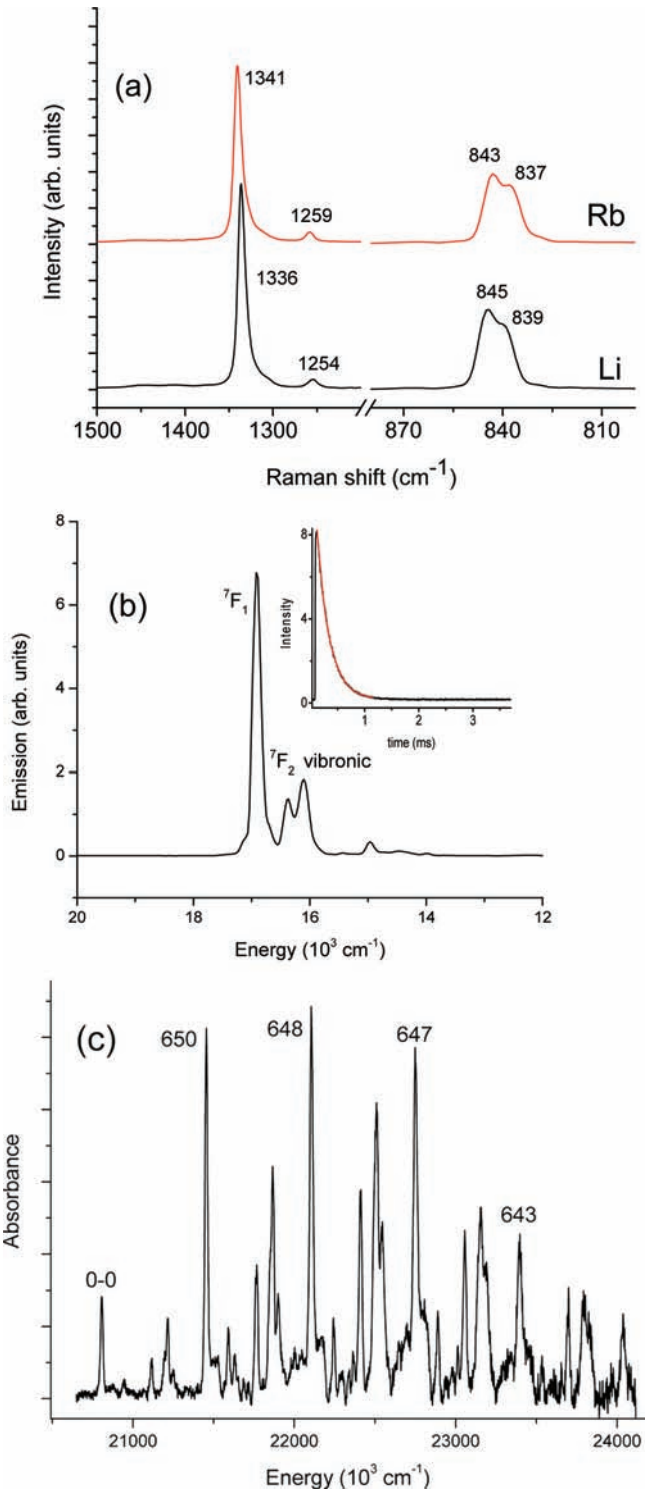

Figure 1. (a) Room temperature Raman spectra of $Cs_2LiEu(NO_2)_6$ and $Rb_2NaEu(NO_2)_6$. The vibrational wavenumbers, in cm^{-1}, are indicated. (b) 440 nm excited room temperature $^5D_0$ visible emission spectrum of $Cs_2NaEu(NO_2)_6$. The terminal multiplets are marked. The inset shows the room temperature decay of $^5D_0$ (λ_{exc} = 467 nm; λ_{em} = 591.3 nm) with the monoexponential fit. (c) 10 K absorption spectrum of $Cs_2NaEu(NO_2)_6$ between 20 650 and 24 100 cm^{-1}. The zero phonon line and successive quanta of the A_g NO_2^- scissoring vibration are marked.

dx.doi.org/10.1021/ic202330h | Inorg. Chem. 2012, 51, 2997−3006

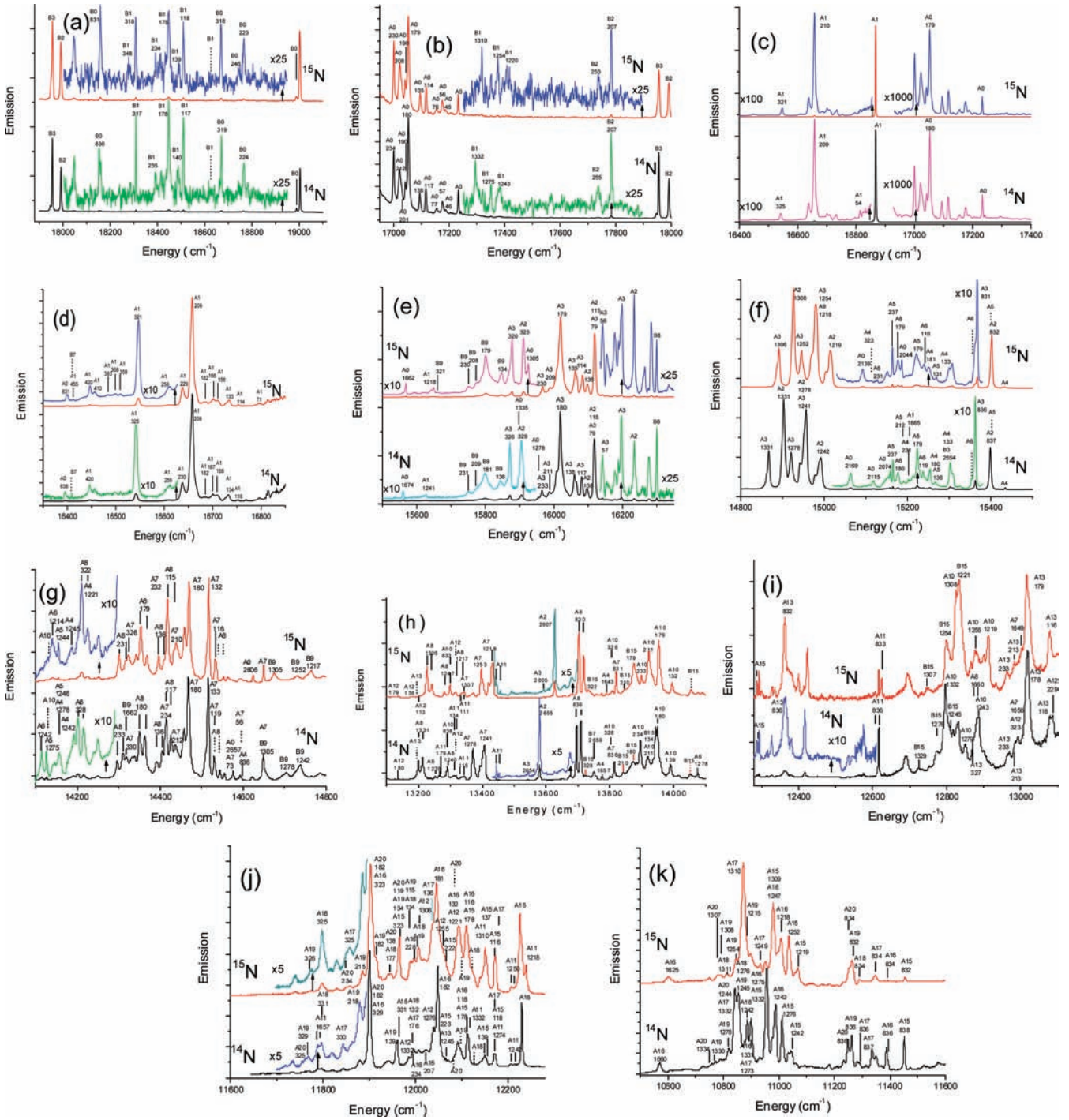

Figure 2. 425 nm excited 3 K visible luminescence spectra of $Cs_2NaEu(^{14}NO_2)_6$ and $Cs_2NaEu(^{15}NO_2)_6$. The spectral bands due to pure electronic transitions are labeled AX for emission from $^5D_0$ or BX from $^5D_1$, where X represents the crystal-field level assignment (Table 3: note that the electronic ground state $^7F_6$ A is designated as 0) of the terminal ^7F_J multiplet term in the transition. Vibronic bands are further labeled by the displacement in cm^{-1} from the respective zero phonon line. Pure electronic transitions that are not observed are indicated by dashed lines, which represent the inferred locations of zero phonon lines.

The 10 K visible absorption spectrum of $Cs_2NaEu(NO_2)_6$ between 20 650 and 24 100 cm^{-1} is shown in Figure 1c. The bands are due to the $^1A_1 \rightarrow {}^3B_1$ transition of NO_2^-, which exhibits a strong progression in the frequency of ~650 cm^{-1}, corresponding to the A_g NO_2^- scissoring mode in the triplet state.

Low-Temperature Luminescence Spectra of Eu^{3+} in Hexanitrito Complexes. Because the zero phonon line of the NO_2^- triplet absorption is at 20 807 cm^{-1}, analysis of energy levels of Eu^{3+} is then restricted to those with lower energy, i.e., $^5D_{0,1}$ and ^7F_J (J = 0–6). The energy-level data set has mostly been deduced from the $^5D_0$ emission spectra, with the aid of some weak emission transitions from $^5D_1$, which are observed at low temperatures. The luminescence spectra of $Cs_2NaEu(NO_2)_6$ and $Cs_2NaEu(^{15}NO_2)_6$ are displayed in Figure 2a–k, those of $Cs_2LiEu(NO_2)_6$ and $Rb_2NaEu(NO_2)_6$ in Figure S1a–k in the Supporting Information, and that of $Cs_2NaY(NO_2)_6$:Eu^{3+}

dx.doi.org/10.1021/ic202330h | Inorg. Chem. 2012, 51, 2997–3006

Table 3. Transition Energies and Calculated and Observed Zero-Phonon-Line MD Intensity Ratios for Europium Hexanitrito Complexes[a]

terminal level		MD relative intensity		energy (cm^{-1})				
		calcd B	obsd	$Cs_2NaEu(^{14}NO_2)_6$	$Cs_2NaEu(^{15}NO_2)_6$	$Cs_2LiEu(NO_2)_6$	$Rb_2NaEu(NO_2)_6$	$Cs_2NaY(NO_2)_6$:Eu
				Initial Level $^5D_0$ A (A)				
0	$^7F_0$ A	0		17 233	17 230	17 232	17 216	17 232
1	$^7F_1$ T	1.0	1.0	16 867	16 867	16 868	16 858	16 867
2	$^7F_2$ T	2×10^{-6}	6×10^{-4}	16 234	16 234	16 235	16 221	16 233
3	$^7F_2$ E	0		16 198	16 198	16 199	16 185	16 198
4	$^7F_3$ T	1×10^{-4}	1×10^{-4}	15 433	15 432	15 434	15 424	15 433
5	$^7F_3$ A	0		15 402	15 400	15 403	15 394	15 402
6	$^7F_3$ T	7×10^{-5}	3×10^{-5}	15 356	15 356	15 357	15 343	15 353
7	$^7F_4$ T	5×10^{-5}	6×10^{-4}	14 649	14 650	14 650	14 646	14 649
8	$^7F_4$ E	0		14 538	14 540	14 537	14 543	14 537
9	$^7F_4$ A	0						14 228
10	$^7F_4$ T	6×10^{-5}	4×10^{-6}	14 129	14 132	14 128	14 110	14 123
11	$^7F_5$ T	1×10^{-4}	6×10^{-6}	13 449	13 451	13 451	13 443	13 447
12	$^7F_5$ T	4×10^{-6}	5×10^{-5}	13 316	13 315		13 312	13 316
13	$^7F_5$ E	0		13 196	13 195	13 198	13 185	13 194
14	$^7F_5$ T	1×10^{-3}						
15	$^7F_6$ A	0		12 289	12 288	12 292	12 275	12 287
16	$^7F_6$ T	2×10^{-3}	8×10^{-5}	12 230	12 226	12 232	12 212	12 229
17	$^7F_6$ T	7×10^{-4}	3×10^{-5}	12 172	12 181	12 175	(12 144)	12 170
18	$^7F_6$ A	0		12 128	12 123	12 130	12 123	12 120
19	$^7F_6$ E	0		12 097	12 100	12 100	12 083	12 093
20	$^7F_6$ T	1×10^{-3}		12 083	12 085	12 085	12 068	12 081
				Initial Level $^5D_1$ T (B)				
15	$^7F_6$ A	2×10^{-3}		14 052	14 054	14 051	14 033	14 049
9	$^7F_4$ A	2×10^{-4}		15 981	15 981	15 978	15 957	15 980
8	$^7F_4$ E	3×10^{-3}		16 299	16 300	16 301	16 287	
7	$^7F_4$ T	2×10^{-3}		16 408				16 408
3	$^7F_2$ E	4	15	17 956	17 956	17 956	17 943	17 955
2	$^7F_2$ T	5	11	17 992	17 991	17 992	17 977	17 990
1	$^7F_1$ T	2×10^{-3}	6×10^{-3}	18 626	18 627	18 627	18 612	18 626
0	$^7F_0$ A	1.0	1.0	18 990	18 989	18 991	18 973	18 989

[a]The transitions from $^5D_0$ and $^5D_1$ are separately normalized.

in Figure S2a–l in the Supporting Information. The labeling of bands is explained in the figure caption. A survey of the 15 K emission spectrum has previously been published for $Cs_2NaEu_{0.01}Y_{0.99}(NO_2)_6$,[15] which shows the relative intensities of spectral features over the visible spectral range.

The emission spectra are particularly complex. This is not only due to the metal–ligand and lattice mode vibronic structure in the $^5D_{J'} \rightarrow {}^7F_J$ ($J' = 0, 1$; $J = 0–6$) transitions but also due to the occurrence of higher-vibrational-energy two-center transitions involving electronic excitation of Eu^{3+} and vibrational excitations of NO_2^-. Two strategies have been put forward in order to unravel and assign the spectral features. First, the large vibrational energy shifts for the $^{14}NO_2$–$^{15}NO_2$ stretching frequencies can provide a firm basis for identification of these modes in vibronic sidebands and the subsequent assignment of zero phonon lines.[15] Second, the low-energy vibronic fingerprint has been identified from the variable-temperature study of the $^5D_0 \rightarrow {}^7F_2$ transition,[16] and use is made of the vibrational frequency changes for $M^I_2M^{II}Eu(NO_2)_6$, where M^I = Cs, Rb; M^{II} = Na, Li, to identify zero phonon lines. However, because of the difficulties in identifying band shifts in congested spectral regions, we now recognize that incorrect assignments have previously been given for the $^5D_0 \rightarrow {}^7F_4$ transition.[15] A reinvestigation of the spectra has been performed at the lower temperature of 3 K in order to more clearly resolve features. Furthermore, use has been made of the energy-level and MD intensity calculations in making the spectral assignments. It is now possible to give a detailed and comprehensive account of the emission spectra, although some assignments still remain tentative, as mentioned in the following description. The zero-phonon-line energies, whether observed or inferred from the vibronic structure, are listed in Table 3, columns 5–9, for the various systems studied. The table also includes a comparison of the calculated and observed MD intensity ratios: relative to $^5D_0 \rightarrow {}^7F_1$ for emission from $^5D_0$ or relative to $^5D_1 \rightarrow {}^7F_0$ for that from $^5D_1$. The ratios have been calculated, as described in the Theoretical Section, using calculation B (Table 3, column 3). The agreement with the experimental results (Table 3, column 4) is subject to an error of an order of magnitude in some cases. For transitions from $^5D_0$, only one transition ($^5D_0$ A $\rightarrow {}^7F_1$ T) is intense and measurement errors arise from a comparison with the intensities of very weak transitions. The errors are attributed to (i) the assumptions used in the calculations and (ii) measurement uncertainties, mainly resulting from baseline errors and overlapping bands, as well as noise levels for weak bands.

dx.doi.org/10.1021/ic202330h | Inorg. Chem. 2012, 51, 2997–3006

The highest-energy emission bands due to Eu^{3+} in panels a of Figures 2 and S1 and S2 in the Supporting Information are due to the $^5D_1 \rightarrow {}^7F_0$ transition, whereas the two intense features at the end of the windows (a) are assigned to $^5D_1 \rightarrow {}^7F_{2,3}$ zero phonon lines (B2 and B3). There are two bands at ~19 000 cm^{-1} that could be associated with the $^5D_1 \rightarrow {}^7F_0$ zero phonon line, with the more intense feature at higher energy. The MD calculation B (Table 3, column 3) indicates that the intensity of the $^5D_1 \rightarrow {}^7F_0$ zero phonon line is considerably weaker than the intensity of $^5D_1 \rightarrow {}^7F_{2,3}$. Furthermore, the derived energy-level structure for ^7F_J levels from the $^5D_1 \rightarrow {}^7F_J$ transitions is only consistent with that from the $^5D_0 \rightarrow {}^7F_J$ transitions if the weaker band is assigned to the $^5D_1 \rightarrow {}^7F_0$ transition (B0). The assignment of the stronger, higher-energy band at ~19 000 cm^{-1} is therefore unclear, and its presence would denote a descent in symmetry from T_h. It may be due to emission from a defect site. High-resolution emission lifetime measurements at low temperature may resolve this assignment.

The $^5D_1 \rightarrow {}^7F_1$ transitions are entirely vibronic in nature and are very weak in intensity. The $^5D_0 \rightarrow {}^7F_0$ transition (A0) commences below 17 250 cm^{-1} (Figures 2 and S1 and S2 in the Supporting Information, panels b), and it is also weak and vibronic in nature. The location of the zero phonon line has been deduced from anti-Stokes luminescence at elevated temperatures,[6,16] and some weak band(s) due to Eu^{3+} ions at defect sites are almost coincident. It is evident from Figure 2b that the energies of low-frequency vibrations are similar in the ^{14}N and ^{15}N spectra but that there are some striking differences in Figure S1b in the Supporting Information for Rb and Li. As mentioned above, these changes facilitate the locations of some other zero phonon lines.

The most dominant band in all spectra is the MD orbitally allowed $^5D_0 \rightarrow {}^7F_1$ (A1) transition near 16 870 cm^{-1} (Figures 2 and S1 and S2 in the Supporting Information, panels c). The vibronic sideband of this transition is very weak (Figures 2 and S1 and S2 in the Supporting Information, panels c and d), and the derived vibrational energies are rather different from those of the $^5D_0 \rightarrow {}^7F_0$ transition because the latter vibrations correspond to ungerade modes, whereas the former are mainly associated with gerade modes in vibrational progressions. The hypersensitive $^5D_0 \rightarrow {}^7F_2$ (T, E) transitions are vibronic in nature and represent the strongest and most clearly identified vibrational sidebands (Figures 2 and S1e in the Supporting Information and subsequent ones; Figure S2d in the Supporting Information and subsequent ones). The $^{14,15}N$ spectra are useful in identifying the contributions from two-center transitions because the ^{14}N scissoring mode (A2 837 and A3 836) shifts to lower energy by ~5 cm^{-1} (Figure 2f), whereas the ^{14}N stretching modes at ~1242, 1278, and 1331 cm^{-1} (Figure 2f) shift by ~25 cm^{-1}. The feature at 1278 cm^{-1} has not been observed in the vibrational spectra. This vibration is assigned to E_g (N−O stretch) from the calculation results in Table 2, and the two-center transition selection rules clearly permit the occurrence of gerade internal anion modes in the emission spectra.[17] Much larger $^{14,15}N$ shifts are observed for some other spectral features. For example, in Figure 2h, the shift of ~49 cm^{-1} for A3 2654 and for A2 2655 identifies these bands as the first members of the A_g (N−O stretch) progression upon the T_u (N−O antisymmetric stretch) vibronic origins. Note that A2 1331 is stronger than A3 1331 (Figure 2f), whereas A2 2655 is very much stronger than A3 2654 (Figure 2h). Other anharmonic progressions that can be identified in the $^{14,15}N$ spectra are some bands based upon the $^5D_0 \rightarrow {}^7F_0$ transition in Figure 2f: A0 2074 (A_g 845 + T_u 1243); A0 2115 (T_u 838 + E_g 1278); A0 2169 (A_g 845 + T_u 1328). Some very weak bands in Figure 2d in the sideband of $^5D_0 \rightarrow {}^7F_1$ are associated with metal−ligand progressions upon vibronic origins.

Several very weak features to low energy of 15 850 cm^{-1} do not exhibit $^{14,15}N$ vibrational shifts and cannot be associated with the sideband of $^5D_0 \rightarrow {}^7F_2$. These bands are present in all spectra (Figures 2 and S1 and S2e in the Supporting Information), and from the energy shifts in the Rb, Li spectra (Figure S1e in the Supporting Information) are alternatively assigned to the sideband of the $^5D_1 \rightarrow {}^7F_4$ A transition. It is interesting that the corresponding transitions from $^5D_0$ cannot be conclusively assigned. Some other luminescence transitions from $^5D_1$ are observed, in addition to those already mentioned, and these are indicated in the figures.

The *SLJ* transition selection rules for vibronic transitions parallel those for Judd forced dipole transitions. Thus, from the initial $^5D_0$ level, the transitions to the terminal *J* values of 2, 4, and 6 are expected to comprise the most vibronic intensity. Hence, the sideband of $^5D_0 \rightarrow {}^7F_3$ is very weak and overlapped by other structures (Figures 2 and S1f and S2e in the Supporting Information). The assignments are confirmed, however, from the lower-energy vibronic transitions involving the N−O stretching modes. The $^5D_0 \rightarrow {}^7F_4$ sideband (panels g in the figures) is more prominent, but only three out of the four crystal-field levels can be readily assigned. The $^7F_4$ crystal-field levels are calculated to lie between 2654 and 3151 cm^{-1} (Table 3), with a gap of 315 cm^{-1} between the E and A levels. Fortunately, the A crystal-field level can be assigned from the sideband of $^5D_1 \rightarrow {}^7F_4$, as described above. It was therefore unexpected that the transitions $^5D_0 \rightarrow {}^7F_4$ E exhibit an apparent splitting of 13 cm^{-1}. This type of situation has previously been encountered in the sidebands of some lanthanide elpasolite systems, notably for $Cs_2NaPrCl_6$,[18] where coupling occurs between the electronic and vibronic levels. In the present case of $Cs_2NaEu(NO_2)_6$, the $^5D_0 \rightarrow {}^7F_4$ T (A7) transition is observed at 14 649 cm^{-1}, whereas the two electronic origins of $^5D_0 \rightarrow {}^7F_4$ E (A8) are inferred to be at 14 531 and 14 544 cm^{-1}. The separation of the A8 barycenter (14 538 cm^{-1}) from A7 is thus 112 cm^{-1}, which is similar to the energy of the T_g Eu−NO_2^- bending vibration, which is 116 cm^{-1} in the Raman spectrum at 300 K.[6] Because the product of $T_g \times T_g$ contains E_g, the pair structure of the transition A8 is assigned to the resonance between $^5D_0 \rightarrow {}^7F_4$ T + T_g and $^5D_1 \rightarrow {}^7F_4$ E. The pair structure is also observed for the two-center vibronic transitions of A8 (Figure 2h). The resonance is not as pronounced in the spectrum of $Rb_2NaEu(NO_2)_6$ (Figure S1h in the Supporting Information), where the electronic and vibrational energies differ from those of $Cs_2NaEu(NO_2)_6$.

The $^5D_0 \rightarrow {}^7F_5$ transitions (A11−A14; Figure 2h−j) are weak in intensity and overlapped by other structures. An apparent splitting of 12 cm^{-1} is observed for the transitions of A11, and this is not readily explained. The assignment of $^5D_0 \rightarrow {}^7F_5$ T (A14) is unclear. There is an unassigned band at 12 691 cm^{-1} in the spectrum of $Cs_2NaEu(^{14}NO_2)_6$ (Figure 2i), which does not exhibit a ^{15}N shift, and it is presumably associated with this transition. A further band at 12 417 cm^{-1} shows a shift of ~7 cm^{-1} and is also unassigned. In Figures 2 and S1j and S2k in the Supporting Information, the $^5D_0 \rightarrow {}^7F_6$ transitions (A15−A20) commence with the vibronic sideband of the A → A transition (A15) and the MD zero phonon line of the transition

dx.doi.org/10.1021/ic202330h | *Inorg. Chem.* 2012, 51, 2997−3006

to the T crystal-field level (A16). The assignment of the highest three $^7F_6$ levels is ambiguous, but a consistent interpretation of the one-center (Figures 2 and S1j and S2k in the Supporting Information) and two-center (Figures 2 and S1k and S2l in the Supporting Information) transitions has been attempted.

The spectrum of $Cs_2NaY(NO_2)_6:Eu^{3+}$ (Figure S2a in the Supporting Information) exhibits some impurity bands due to the strongest transition of Tb^{3+}, $^5D_4 \rightarrow {}^7F_5$, and these are marked. There is also an unidentified species, giving rise to the bands marked X and X + 835 in this spectrum. The spectrum in Figure S2l in the Supporting Information exhibits an artifact due to the superposition of an interference fringe.

Crystal-Field Analysis of Energy Levels. Spectral analysis has enabled the determination of 22 of the ^7F_J (J = 0−6) and ^5D_J (J = 0, 1) energy levels of Eu^{3+} in various hexanitrito complexes. Table 3 shows that the transition energies, and hence the derived energy levels, are very similar for all of these systems, with $Rb_2NaEu(NO_2)_6$ exhibiting the greatest differences. In view of the similar energy-level data sets, we performed the data fitting only for the $Cs_2NaEu(NO_2)_6$ data set, as listed in Table 4. The energy levels were fitted by the parametric Hamiltonian, employing the parameters listed in Table 5. The seven crystal-field, Slater, and spin−orbit parameters were varied, whereas other parameters were held at the values for $Cs_2NaEuCl_6$ in calculations A and B. The fittings provide a reasonable mean deviation of ∼20 cm^{-1}, and the crystal-field and spin−orbit parameters from the two calculations are comparable. The calculated and experimental energies are compared in Table 3, and calculation B gives a slightly better agreement with experiment.

Table 4. Calculated (E_{calc}) and Experimentally Derived (E_{expt}) Energy Levels (in cm^{-1}) of Eu^{3+} in $Cs_2NaEu(NO_2)_6$[a]

label	$^{2S+1}L_J$ Γ	E_{expt}	E_{calc} (A)	$E_{expt} - E_{calc}$ (A)	E_{calc} (B)	$E_{expt} - E_{calc}$ (B)
0	$^7F_0$ A	0	0	0	0	0
1	$^7F_1$ T	365	375	−10	374	−9
2	$^7F_2$ T	999	1004	−5	1009	−10
3	$^7F_2$ E	1035	1063	−28	1050	−15
4	$^7F_3$ T	1800	1792	8	1786	14
5	$^7F_3$ A	1831	1832	−1	1822	9
6	$^7F_3$ T	1877	1926	−49	1921	−44
7	$^7F_4$ T	2583	2624	−41	2611	−28
8	$^7F_4$ E	2694	2687	8	2691	3
9	$^7F_4$ A	3009	3002	7	3000	9
10	$^7F_4$ T	3104	3151	−47	3149	−45
11	$^7F_5$ T	3784	3786	−2	3771	13
12	$^7F_5$ T	3917	3925	−8	3942	−25
13	$^7F_5$ E	4037	4032	5	4039	−2
14	$^7F_5$ T		4195		4202	
15	$^7F_6$ A	4940	4920	20	4928	12
16	$^7F_6$ T	5003	4992	11	5001	2
17	$^7F_6$ T	5061	5047	14	5057	4
18	$^7F_6$ A	5105	5109	−4	5120	−1
19	$^7F_6$ E	5136	5114	22	5106	21
20	$^7F_6$ T	5150	5118	32	5115	30
A	$^5D_0$ A	17 233	17 234	−1	17 235	−2
B	$^5D_1$ T	18 990	18 991	0	18 994	−4

[a]The fixed parameters in calculations A and B were taken from refs 12 and 13, respectively.

Table 5. Parameter Values (in cm^{-1}, Except for N and n_p, Which Are Dimensionless) Employed in the Energy-Level Calculations

parameter	calcd A value[a]	calcd B value[b]
E_{exc}	[100 000]	[100 000]
F^2	84 335	82 149
F^4	59 785	62 928
F^6	41 019	42 804
$\zeta(4f)$	1330	1331
α	[16.8]	[27.70]
β	[−640]	[−1272]
γ	[1750]	[1461]
M_{tot}	[2.38]	[2.13]
P_{tot}	[245]	[195]
B_{40}	−433	−327
B_{60}	−304	−260
B_{62}	−1599	−1680
T^2	[370]	[278]
T^3	[40]	[40]
T^4	[40]	[40]
T^6	[−330]	[−546]
T^7	[380]	[244]
T^8	[370]	[241]
N	22	22
n_p	7	7
δ_1	25.4	22.9
δ_2	21.0	18.9

[a]Square brackets indicate that the parameter was fixed at the value for $Cs_2NaEuCl_6$ from ref 12. [b]Square brackets indicate that the parameter was fixed at the value for $Cs_2NaEuCl_6$ from ref 13.

$$\delta_1 = \sqrt{\frac{(E_{calc} - E_{expt})^2}{N - n_p}}$$

$$\delta_2 = \sqrt{\frac{(E_{calc} - E_{expt})^2}{N}}$$

For the lanthanide hexachloroelpasolites, the crystal-field parameter B_{40} is roughly an order of magnitude greater than B_{60}.[13] Table 5 shows that these parameters are of the same order in the present case. The parameter B_{40} has been shown to depend strongly on the Ln−ligand distance. The ratio of the inverse fifth powers of the Eu−Cl and Eu−O distances is ∼0.7, which would reduce B_{40} from the value in the chloride system to ∼1450 cm^{-1} in $Cs_2NaEu(NO_2)_6$, compared to the value in $Cs_2NaEuCl_6$, so that the substitution of 12-coordinated oxygen for 6-coordinated chlorine has a more dramatic impact. The variation of B_{40} and B_{60} across the Ln^{3+} series for the $Cs_2NaLn(NO_2)_6$ compounds will be of interest because both parameters herein are less negative than those for Ln = Pr.[4] For both Ln = Pr and Eu, the parameter B_{62} dominates B_{40} and B_{60} (Table 5).

Although there are no other reported lanthanide ion systems with T_h symmetry that are available to our knowledge for comparison with the present study, the rare-earth double nitrate $Eu_2Zn_3(NO_3)_{12}\cdot 24H_2O$ (abbreviated as EuDN hereafter) has some similarities. The Eu^{3+} ion in EuDN is surrounded by six bidentate nitrate groups in a distorted icosahedral geometry. The crystal field is therefore predominantly

dx.doi.org/10.1021/ic202330h | Inorg. Chem. 2012, 51, 2997−3006

Table A1. Character Table for the T_h Point Group. ($T_h = T \times i$). Note that the degenerate singlet representations $\Gamma_{2,3}$ are denoted as E in this study for convenience. ($\omega = \exp(2\pi i/3)$)

T_h	E	$4C_3$	$4C_3^2$	$3C_2$	i	$4S_6$	$4S_6^5$	$3\sigma_h$	bases
A_g	1	1	1	1	1	1	1	1	$x^2 + y^2 + z^2$
E_g	$\{^1_1$	$\{^{\varepsilon}_{\varepsilon^*}$	$\{^{\varepsilon^*}_{\varepsilon}$	$\{^1_1$	$\{^1_1$	$\{^{\varepsilon}_{\varepsilon^*}$	$\{^{\varepsilon^*}_{\varepsilon}$	$\{^1_1$	$(2z^2 - x^2 - y^2); x^2 - y^2$
T_g	3	0	0	−1	1	0	0	−1	$(R_x,R_y,R_z); (xz, yz, xy)$
A_u	1	1	1	1	−1	−1	−1	−1	
E_u	$\{^1_1$	$\{^{\varepsilon}_{\varepsilon^*}$	$\{^{\varepsilon^*}_{\varepsilon}$	$\{^1_1$	$\{^{-1}_{-1}$	$\{^{-\varepsilon}_{-\varepsilon^*}$	$\{^{-\varepsilon^*}_{-\varepsilon}$	$\{^{-1}_{-1}$	
T_u	3	0	0	−1	1	0	0	−1	(x,y,z)

tetrahedral (T_h) with a distortion to C_3. The S_6 rotation−inversion axis does not exist in the EuDN molecular ion, and the principal symmetry axis is C_3. The approximation to C_{3v} symmetry enabled the fitting of crystal-field levels by a parametrized Hamiltonian with six real crystal-field parameters by Görller-Walrand et al.,[19] who reported the absorption and emission spectra of EuDN. The sixth-ranked crystal-field parameter B_{63} was of the greatest magnitude (=−1557 cm^{-1}), and $131B_{40} = B_{60}$. The deviation from T_h symmetry necessitated the introduction of the second-ranked parameter B_{20}, which leads to the splitting of T (T_h) levels in $^7F_1$, for example, to A + E (C_{3v}) crystal-field levels. By taking into account the symmetries of the crystal-field levels in EuDN[19] and converting from C_{3v} to T_h by locating the barycenters of the A + E (C_{3v}) levels, the following energy-level data set (expressed in cm^{-1}) results for the $^7F_{1,2,3}$ and $^5D_{0,1}$ multiplets of EuDN: $^7F_0$, 0; $^7F_1$, 364; $^7F_2$, 1001, 1056; $^7F_3$, 1803,1812, 1947; $^5D_0$, 17 247; $^5D_1$, 19 000. These energies are independent of the sixth-ranked parameters and are remarkably similar to those in Table 4, thereby demonstrating their similarity in the coordination type and geometry. The major difference in the spectra of EuDN and $Cs_2NaEu(NO_2)_6$ is that pure electronic transitions can gain forced electric-dipole intensity in the former case.

Roser and Corruccini[3] have investigated the temperature-dependent magnetic susceptibilities of some $Cs_2NaLn(NO_2)_6$ systems but did not study Ln = Eu. The ground state of the present Eu^{3+} system is $^7F_0$ A, and because $\langle ^7F_0||\mathbf{L} + 2\mathbf{S}||^7F_0\rangle = 0$, the magnetic susceptibility in the first order of the perturbation theory is zero. The lowest excited state is $^7F_1$ T at 365 cm^{-1}, which is much larger than kT, so that the magnetic susceptibility in the second order of the perturbation theory is also near zero at temperatures lower than 300 K, for example.

CONCLUSIONS

The study of the electronic spectra of Eu^{3+} in $Cs_2NaEu(NO_2)_6$ is restricted to $^5D_1$ and the lower multiplets because of the absorption bands of the NO_2^- anion above 20 000 cm^{-1}. An attempt has been made to unravel the complexity of the luminescence spectra by using low temperatures, nitrogen isotopic substitution, and cation substitution. The understanding of the vibrational behavior of this system was a necessary prerequisite for attempting the interpretation of the luminescence spectra, and this was accomplished by DFT calculations. Emission has been reported from both of the $^5D_0$ and $^5D_1$ multiplet terms. Most of the emission bands have been assigned to MD-allowed zero phonon lines, ungerade metal−ligand vibrations, and lattice and internal cation modes. The internal cation modes are particularly intense in the sideband of the hypersensitive $^5D_0 \rightarrow {}^7F_2$ transition.

The energy-level fitting of 22 levels shows a larger mean deviation than that for the case of the elpasolite $Cs_2NaEuCl_6$.[12,13] The sixth-ranked parameter B_{62} dominates other crystal-field parameters, just as for Pr^{3+} in $Cs_2NaPr(NO_2)_6$.[4] The two energy-level calculations provide a consistent ordering of the symmetry representations of the crystal-field levels, with the exception of $^7F_6$ A and $^7F_6$ E, which are fairly close in energy.

APPENDIX

Tables A1−A3 are given.

Table A2. MD Transition Activity for Eu^{3+} in the Point Group T_h

initial state/final state	A_g	E_g	T_g
A_g			√
E_g			√
T_g	√	√	√

Table A3. Vibronic Activity for Eu^{3+} in the Point Group T_h

initial state/final state	A_g	E_g	T_g
A_g	T_u	T_u	$E_u + A_u + T_u$
E_g	T_u	T_u	$E_u + A_u + T_u$
T_g	$E_u + A_u + T_u$	$E_u + A_u + T_u$	$E_u + A_u + T_u$

ASSOCIATED CONTENT

Supporting Information

Emission spectra of $Cs_2LiEu(NO_2)_6$ and $Rb_2NaEu(NO_2)_6$ (Figure S1), $Cs_2NaY(NO_2)_6$:Eu^{3+} (1 atom %; Figure S2), and room temperature excitation spectrum of $Cs_2NaEu(NO_2)_6$ (Figure S3). This material is available free of charge via the Internet at http://pubs.acs.org.

AUTHOR INFORMATION

Corresponding Author

*E-mail: peter.a.tanner@gmail.com. Tel.: (852) 90290610.

ACKNOWLEDGMENTS

Financial support from the National Science Foundation of China (Grant 11174005) is gratefully acknowledged by L.N.

REFERENCES

(1) Barnes, J. C.; Al-Rasoul, K.; Harkins, P. *J. Chem. Soc. Pak.* **1980**, *2*, 9.
(2) Caulton, K. G.; Fenske, R. F. *Inorg. Chem.* **1967**, *6*, 562.
(3) Roser, M. R.; Corruccini, L. R. *Phys. Rev. B* **1990**, *41*, 2359.
(4) Li, W.; Ning, L.; Faucher, M. D.; Tanner, P. A. *Inorg. Chem.* **2011**, *50*, 9004.
(5) Barnes, J. C.; Peacock, R. D. *J. Chem. Soc. A* **1971**, 558.
(6) Bünzli, J.-C.; Petaud, G. S.; Moret, E. *Spectrosc. Lett.* **1999**, *32*, 155.
(7) Kresse, G.; Furthmüller, J. *Phys. Rev. B* **1996**, *54*, 11169.
(8) Perdew, P.; Burke, K.; Ernzerhof, M. *Phys. Rev. Lett.* **1996**, *77*, 3865.
(9) Blöchl, P. E. *Phys. Rev. B* **1994**, *50*, 17953.

(10) Kresse, G.; Joubert, D. *Phys. Rev. B* **1999**, *59*, 1758.
(11) Liu, G. K. In *Spectroscopic Properties of Rare Earths in Optical Materials*; Liu, G. K., Jacquier, B., Eds.; Springer: Berlin, 2005; pp 1−89.
(12) Tanner, P. A.; Ravi Kanth Kumar, V. V.; Jayasankar, C. K.; Reid, M. F. *J. Alloys Compd.* **1994**, *215*, 349.
(13) Duan, C.-K.; Tanner, P. A. *J. Phys. Chem. A* **2010**, *114*, 6055.
(14) Görller-Walrand, C.; Binnemans, K. In *Handbook on the Physics and Chemistry of Rare Earths*; Gschneidner, K. A., Jr., Eyring, L., Eds.; Elsevier: Amsterdam, The Netherlands, 1998; Chapter 167, pp 101−264.
(15) Li, W.; Tanner, P. A. *Inorg. Chem.* **2010**, *49*, 6384.
(16) Li, W.; Tanner, P. A. *Chem. Phys. Lett.* **2010**, *494*, 50.
(17) Dexpert-Ghys, J.; Auzel, F. *J. Chem. Phys.* **1984**, *80*, 4003.
(18) Tanner, P. A. *Mol. Phys.* **1986**, *57*, 697.
(19) Görller-Walrand, C.; Hendrickx, I.; Fluyt, L.; Gos, M. P.; D'Olieslager, J.; Blasse, G. *J. Chem. Phys.* **1992**, *96*, 5650.